

ADAPTIVE TIME-STEPPING SCHEMES FOR THE SOLUTION OF THE POISSON-NERNST-PLANCK EQUATIONS

DAVID YAN , M. C. PUGH*, AND F. P. DAWSON†

Abstract. The Poisson-Nernst-Planck equations with generalized Frumkin-Butler-Volmer boundary conditions (PNP-FBV) describe ion transport with Faradaic reactions, and have applications in a number of fields. In this article, we develop an adaptive time-stepping scheme for the solution of the PNP-FBV equations based on two time-stepping methods: a fully implicit (BDF2) method, and an implicit-explicit (SBDF2) method. We present simulations under both current and voltage boundary conditions and demonstrate the ability to simulate a large range of parameters, including any value of the singular perturbation parameter ϵ . When the underlying dynamics is one that would have the solutions converge to a steady-state solution, we observe that the adaptive time-stepper based on the SBDF2 method produces solutions that “nearly” converge to the steady state and that, simultaneously, the time-step sizes stabilize to a limiting size dt_∞ . In the companion to this article [1], we linearize the SBDF2 scheme about the steady-state solution and demonstrate that the linearized scheme is conditionally stable. This conditional stability is the cause of the adaptive time-stepper’s behaviour. While the adaptive time-stepper based on the fully-implicit (BDF2) method is not subject to such time-step constraints, the required nonlinear solve yields run times that are significantly longer.

Key words. Poisson-Nernst-Planck Equations, Semi-Implicit Methods, IMEX Methods, BDF2, SBDF2, Adaptive Time Stepping, Conditional Linear Stability

AMS subject classifications. 65M12, 65Z05, 78A57

1. Introduction. The Poisson-Nernst-Planck (PNP) equations describe the transport of charged species subject to diffusion and electromigration. They have wide applicability in electrochemistry, and have been used to model a number of different systems, including porous media [2, 3, 4, 5], microelectrodes [6, 7], ion-exchange membranes [8, 9], electrokinetic phenomena [10, 11, 12], ionic liquids [13, 14], electrochemical thin films [15, 16, 17], fuel cells [18], supercapacitors [19], and more.

The one-dimensional, nondimensionalized PNP equations for a media with 2 mobile species is

$$(1) \quad \frac{\partial c_\pm}{\partial t} = -\frac{\partial}{\partial x} \left[-\frac{\partial c_\pm}{\partial x} - z_\pm c_\pm \frac{\partial \phi}{\partial x} \right], \quad t > 0, x \in (0, 1),$$

$$(2) \quad -\epsilon^2 \frac{\partial^2 \phi}{\partial x^2} = \frac{1}{2} (z_+ c_+ + z_- c_-), \quad x \in (0, 1),$$

where c_\pm and z_\pm are the concentration and charge number of the positive/negative ion, ϕ is the potential and ϵ is the ratio of the Debye screening length to the interelectrode width L . We consider a model in which the anion has no charge-transfer reactions at the electrode: c_- has zero flux boundary conditions. The cation is assumed to have a reaction at the electrode involving the transfer of one electron; this is modelled using

*Department of Mathematics, University of Toronto (mpugh@math.utoronto.ca)

†Department of Electrical and Computer Engineering, University of Toronto

generalized Frumkin-Butler-Volmer (FBV) boundary conditions:

$$(3) \quad -\left(-\frac{\partial c_-}{\partial x} - c_- \frac{\partial \phi}{\partial x}\right) \Big|_{x=0} = \left(-\frac{\partial c_-}{\partial x} - c_- \frac{\partial \phi}{\partial x}\right) \Big|_{x=1} = 0$$

$$(4) \quad -\left(-\frac{\partial c_+}{\partial x} - c_+ \frac{\partial \phi}{\partial x}\right) \Big|_{x=0} = F(t) := 4k_{c,a} c_+(0, t) e^{-0.5 \Delta \phi_{\text{left}}} - 4j_{r,a} e^{0.5 \Delta \phi_{\text{left}}},$$

$$(5) \quad \left(-\frac{\partial c_+}{\partial x} - c_+ \frac{\partial \phi}{\partial x}\right) \Big|_{x=1} = G(t) := 4k_{c,c} c_+(1, t) e^{-0.5 \Delta \phi_{\text{right}}} - 4j_{r,c} e^{0.5 \Delta \phi_{\text{right}}},$$

where $k_{c,a}$, $k_{c,c}$, $j_{r,a}$, and $j_{r,c}$ are reaction rate parameters; the second letter in the subscripts (a and c) refer to the anode and cathode, respectively. Equations (4)–(5) model the electrodeposition reaction



where M represents the electrode material. There is a compact layer of charge, called the Stern layer, that occurs in the electrolyte next to an electrode surface [20, 21]. In equations (4)–(5), $\Delta \phi_{\text{left}}$ and $\Delta \phi_{\text{right}}$ refer to the potential differences across the Stern layers that occur at the anode and cathode respectively. Specifically,

$$(7) \quad \Delta \phi_{\text{left}} = \phi_{\text{anode}} - \phi(0, t) = -\phi(0, t), \quad \Delta \phi_{\text{right}} = \phi_{\text{cathode}} - \phi(1, t) = v(t) - \phi(1, t)$$

where the potential at the anode has been set to zero and $v(t)$ denotes the potential at the cathode.

The Poisson equation (2) uses a mixed (or Robin) boundary condition [15, 16, 17],

$$(8) \quad -\epsilon \delta \frac{\partial \phi}{\partial x} \Big|_{x=0} = \Delta \phi_{\text{left}} := -\phi(0, t),$$

$$(9) \quad +\epsilon \delta \frac{\partial \phi}{\partial x} \Big|_{x=1} = \Delta \phi_{\text{right}} := v(t) - \phi(1, t),$$

where δ is the ratio of the compact layer thickness to L . Finally, there is an ODE which ensures conservation of electrical current at the electrode [22, 23],

$$(10) \quad -\frac{\epsilon^2}{2} \frac{d}{dt} \phi_x(1, t) = j_{\text{ext}}(t) - [k_{c,c} c_+(1, t) e^{-0.5 \Delta \phi_{\text{right}}} - j_{r,c} e^{0.5 \Delta \phi_{\text{right}}}],$$

where $j_{\text{ext}}(t)$ is the current through the device. We refer to the PNP equations with the generalized Frumkin-Butler-Volmer boundary conditions as the PNP-FBV system.

Considering more than two charged species or reactions involving the transfer of more than one electron is a straight-forward generalization [24, 25]. If the model is extended to include adsorption effects at the electrodes, there would be an additional ODE describing the dynamics of the fraction of surface coverage for each electrode [26]. If, in addition, the model included temperature and heat transport, there would be another PDE for the temperature [26]. In this work however, we limit ourselves to just the PNP-FBV system of equations.

The device is operated in two regimes — either the current or the voltage at the cathode is externally controlled. If the voltage at the cathode, $v(t)$, is externally controlled then the the PNP-FBV system (1)–(2) with boundary conditions (3)–(5) and (7)–(9) are numerically solved, determining c_{\pm} and ϕ . The current is found *a posteriori* using equation (10). If the current, $j_{\text{ext}}(t)$, is externally controlled, then

equation (10) is part of the PNP-FBV system and the ODE is numerically solved along with the PDEs, determining c_{\pm} , ϕ , and $\phi_x(1, t)$ simultaneously. The voltage $v(t)$ is then found *a posteriori*.

Though many workers in the field have approximated solutions to the PNP-FBV system using asymptotic methods [27, 28], a numerical method is needed to obtain a full solution. A key mathematical aspect of the PNP-FBV system is that the parameter ϵ acts as a singular perturbation to the system and results in the formation of boundary layers [29]. This makes numerical simulation of the PNP-FBV system especially challenging.

In general, there are several properties of a numerical method that need to be established so as to allow the solver for the Poisson-Nernst-Planck equations to be stable and provide accurate results. The first is a nonuniform mesh in space, which is useful because the potential and concentration distributions near the electrode can change significantly over short distances. The mesh near the boundaries should be finer than the mesh in the middle of the domain, where the concentration and potential are nearly constant. Secondly, many electrochemical systems of interest are subject to sudden changes of forcing, with long periods of relaxation with constant or no forcing in between. This, along with the transient dynamics driven by the initial data, gives the problem more than one timescale.

One of the first contributions to the field of time-stepping methods for the Poisson-Nernst-Planck equations, was by Cohen and Cooley [30], who used an explicit time-stepping method with predictor-corrector time-step refinement to solve the electroneutral equations with constant current. The next contribution was by Sandifer and Buck [31], who solved a system of equations with time-independent Nernst-Planck equations with constant current and an implicit, iterative method to step the displacement field. Brumleve and Buck [32] solved the full PNP equations with Chang-Jaffe boundary conditions using Backward Euler time-stepping. In Brumleve and Buck's method, time-steps were allowed to be variable, but were not adjusted during each step; the method given in the original publication still sees use in more modern work [33]. Murphy et. al. [34] solved the full PNP-FBV system with adaptive steps by treating the discretized parabolic-elliptic system as a differential-algebraic system of ODE's and algebraic equations, and used a variable-order Gear's method [35]. It is also worth mentioning here the work of Scharfetter and Gummel [36], who gave a numerical method to solve the drift-diffusion equations (an analogue of the PNP equations in semiconductor physics) using Crank-Nicolson time-stepping.

A recent work where the time-dependent PNP equations are solved is Soestbergen, Biesheuvel and Bazant [23] (with FBV) who used the commercial finite element software COMSOL, which uses BDF and the generalized- α method [37]. Another is Britz and Strutwolf [38], who simulate a liquid junction using BDF with constant time-steps. Britz [39] also outlines various explicit and implicit multistep methods in his book on computational solutions to the PNP equations. Our present work differs from previous attempts (notably Murphy et. al.) by using a splitting method for the parabolic-elliptic system (1)–(2) rather than treating them as a system of DAE's, and differs from other modern computational methods [40] by controlling time-steps adaptively.

In this article, we develop and test adaptive time-steppers for the PNP-FBV system with error control. This will allow the time-stepper to automatically detect changes in time scales and vary the step size accordingly. One of the adaptive time-steppers is based on a second-order variable step-size, semi-implicit, backward differentiation formula (Variable Step-size Semi-implicit Backwards Differentiation

Formula, or VSSBDF2 [41]). Its constant step-size counterpart (Semi-implicit Backwards Differentiation Formula, or SBDF2) is used as a time-stepping scheme in a variety of fields in science, engineering and computational mathematics. Axelsson et. al. [42], for example, used SBDF2 with constant steps to solve the time-dependent Navier-Stokes equations. Lecoanet et. al. [43] used a similar method to model combustion equations in stars, and Linde, Persson and Sydow [44] used it to solve the Black-Scholes equation in computational finance. An example of an adaptive SBDF2 time-stepping scheme can be found in Rosam, Jimack and Mullis [45], who use it to study a problem in binary alloy solidification. In their Figure 4, they appear to show time-steps relaxing to a constant value (i.e. thresholding), but the reason is not given: they report that it is related to the tolerance set in the adaptive time-stepper.

The other adaptive time-stepper we develop is based on a second-order Variable Step-size, fully implicit, Backward Differentiation Formula (VSBDF2). Its constant step-size counterpart (BDF2) has the advantage of being unconditionally stable when applied to linear systems that have asymptotically stable steady states. An example of VSBDF2 is Eckert et. al. [46], who use it to model electroplasticity; their scheme is fully implicit and they do not report any kind of instability or time step constraint. However, for nonlinear problems, this numerical stability comes at the cost of needing to perform a computationally expensive nonlinear solve at each time-step.

We find that when the underlying dynamics of the PNP-FBV system are such that solutions converge to a steady-state solution, the VSSBDF2 adaptive timestepper does not take larger and larger time-step sizes until reaching a user-defined maximum time-step size dt_{\max} . In fact, we observe that the solution gets close to, but fails to converge to, the stable steady state and, simultaneously, the time-step sizes stabilize at a limiting step size dt_{∞} . We also observe this limiting-time-step-size behaviour in simulations of systems that have rapidly changing voltage or current forcing as long as the times of rapid change are sufficiently separated in time that the solution is relaxing to a steady state in the time intervals between the rapid changes.

In comparison, when the underlying solution is relaxing to a steady-state solution, the VSBDF2 adaptive time-stepper can take time-steps to be arbitrarily large, up to a user-specified maximum time-step dt_{\max} . Although the time-steps can be large, we find that the run time for the fully implicit scheme is longer than for the semi-implicit scheme, despite its stability constraint, due to the nonlinear solve necessary at each time-step.

In the companion article [1] we perform a linear stability analysis of the SBDF2 scheme about the steady-state solution, and demonstrate that the scheme is conditionally stable with a step size stability threshold dt^* . We demonstrate that it is this underlying stability constraint that causes the VSSBDF2 adaptive timestepper to have a limiting time-step size, and present numerical evidence that $dt_{\infty} = dt^*$. We find that varying the tolerance set in the adaptive time-stepper does not affect the limiting step size dt_{∞} .

While the methods we present in the current work are directly applicable to achieving faster and more accurate solutions of the PNP-FBV equations, they are also relevant in general to systems of coupled parabolic-elliptic equations. Also, the stability analysis in the companion paper could also be used for any multistep implicit-explicit scheme.

This article is structured as follows. Subsection 2.1 presents the temporal discretization and Subsections 2.4 and 2.5 present the spatial discretization. Subsections 2.2–2.3 present the adaptive stepping and error control algorithms. Subsection 2.6 discusses how to apply the time-stepping scheme to the PNP-FBV system. In Section

3, we apply the scheme to the PNP-FBV system and study its performance including the effect of the singular perturbation parameter ϵ . In Appendix A we present the derivation of the local truncation error formula.

2. The Numerical Method.

2.1. Time-Stepping. Multistep schemes such as backwards differentiation formulae, Adams-Basforth, and Crank-Nicolson methods have long been applied in computational fluid mechanics to time step advection-diffusion ODEs (see Chapter 4.4 of [47]) where both the diffusion and advection terms are linear.

Semi-implicit, or implicit-explicit schemes, are useful when ODEs or contain both linear stiff terms and nonlinear terms which are difficult to handle using implicit methods. Consider the ODE $u' = f(u) + g(u)$ where $f(u)$ is a nonlinear term and $g(u)$ is a stiff linear term. Given u^{n-1} at time $t^{n-1} = t^n - dt_{\text{old}}$ and u^n at time t^n , u^{n+1} at time $t^{n+1} = t^n + dt_{\text{now}}$ is determined via

$$(11) \quad \text{SBDF2: } \frac{1}{dt} \left(\frac{3}{2}u^{n+1} - 2u^n + \frac{1}{2}u^{n-1} \right) = 2f(u^n) - f(u^{n-1}) + g(u^{n+1}),$$

where the superscript notation denotes time levels: u^n approximates $u(t^n)$ (see, for example, [48, 49]).

Our VSSBDF2 adaptive timestepper is based on a second-order variable step-size implicit-explicit backwards differencing formula, introduced by Wang and Ruuth [41], as a generalization of the SBDF2 scheme:

$$(12) \quad \text{VSSBDF2: } \frac{1}{dt_{\text{now}}} \left(\frac{1+2\omega}{1+\omega}u^{n+1} - (1+\omega)u^n + \frac{\omega^2}{1+\omega}u^{n-1} \right) = (1+\omega)f(u^n) - \omega f(u^{n-1}) + g(u^{n+1}),$$

where $\omega = dt_{\text{now}}/dt_{\text{old}}$. We use this scheme for (1) with term $c_{\pm,xx}$ implicit (like g) and the term $z_{\pm}(c_{\pm}\phi_x)_x$ explicit (like f). We chose this scheme because the PDEs for the concentration (1) are advection diffusion equations; this scheme was shown to have favorable stability properties compared to the other IMEX schemes based on numerical experiments on Burger's equation [41].

A one-step semi-implicit scheme is used for the first time-step

$$(13) \quad \frac{1}{dt} (u^1 - u^0) = f(u^0) + g(u^1).$$

To compare the semi-implicit schemes to fully implicit schemes, we also consider the second-order backwards differencing formula, BDF2,

$$(14) \quad \text{BDF2: } \frac{1}{dt} \left(\frac{3}{3}u^{n+1} - 2u^n + \frac{1}{2}u^{n-1} \right) = g(u^{n+1}).$$

Our VSBDF2 adaptive timestepper is based on the second-order variable step-size backwards differencing formula which is a generalization of the BDF2 scheme:

$$(15) \quad \text{VSBDF2: } \frac{1}{dt_{\text{now}}} \left(\frac{1+2\omega}{1+\omega}u^{n+1} - (1+\omega)u^n + \frac{\omega^2}{1+\omega}u^{n-1} \right) = g(u^{n+1}),$$

where $\omega = dt_{\text{now}}/dt_{\text{old}}$. Here, g represents $c_{\pm,xx} + z_{\pm}(c_{\pm}\phi_x)_x$. Backward Euler is used for the first time-step

$$(16) \quad \frac{1}{dt} (u^1 - u^0) = g(u^1).$$

2.2. Error Approximation and Extrapolation. If one is using a non-adaptive time-stepper then the time steps t^n , $n = 0, 1, \dots$ are chosen before computing u^n , $n = 0, 1, \dots$. An adaptive time-stepper chooses the time-step size dt_{now} based on already-computed quantities. For example, using the values u^{n-1} , $u^{n-\frac{1}{2}}$ and u^n at times $t^n - dt_{\text{old}}$, $t^n - dt_{\text{old}}/2$ and t^n we choose a time-step size dt_{now} so that the local truncation error (LTE) is “small enough” but not “too small”. This is done as follows. First, we choose a candidate time-step: $dt_{\text{now}} = dt_{\text{old}}$, for example. We then take one “coarse” step from $t^n - dt_{\text{old}}$ and t^n to $t^n + dt_{\text{now}}$, using u^{n-1} and u^n to create u_c^{n+1} . Next, we take one “fine” step from $t^n - dt_{\text{old}}/2$ and t^n to $t^n + dt_{\text{now}}/2$, using $u_f^{n-\frac{1}{2}}$ and u^n to create $u_f^{n+\frac{1}{2}}$ and take a second fine step from t^n and $t^n + dt_{\text{now}}/2$, using u^n and $u_f^{n+\frac{1}{2}}$ to create u_f^{n+1} . We use u_c^{n+1} and u_f^{n+1} to estimate the local truncation error; if the error is acceptable we advance in time. If the error is unacceptable we choose a new dt_{now} and try again. This scheme is shown in Figure 1. Note that in the figure, $dt_{\text{now}} > dt_{\text{old}}$; this would happen in the first attempt if the local truncation error was “too small”. Given the two approximations u_c^{n+1} and u_f^{n+1} of the solution

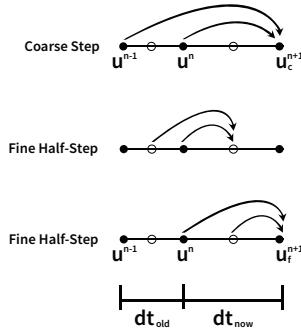


Fig. 1: Coarse/fine time-stepping scheme. First a coarse time-step uses u^{n-1} and u^n to create u_c^{n+1} . Then a fine time-step uses $u_f^{n-\frac{1}{2}}$ and u^n to create $u_f^{n+\frac{1}{2}}$ and another fine time-step uses u^n and $u_f^{n+\frac{1}{2}}$ to create u_f^{n+1} . In the diagram, open circles indicate values from fine half-steps.

at time $t^n + dt_{\text{now}}$, one can use them to approximate the local truncation error (see Appendix A):

$$(17) \quad \epsilon_c^{n+1} = \frac{8(dt_{\text{old}} + dt_{\text{now}})}{7dt_{\text{old}} + 5dt_{\text{now}}} (u_c^{n+1} - u_f^{n+1}) \approx u_c^{n+1} - u(t^{n+1}).$$

We use this approximation of ϵ_c when testing whether to use dt_{now} or to coarsen or refine it. If dt_{now} has been accepted, we can then use u_f^{n+1} and u_c^{n+1} to construct an approximation u^{n+1} which has smaller truncation error. Specifically, u^{n+1} is a linear combination of the form $u^{n+1} = \alpha u_c^{n+1} + \beta u_f^{n+1}$ with coefficients

$$(18) \quad \alpha = -\frac{dt_{\text{old}} + 3dt_{\text{now}}}{7dt_{\text{old}} + 5dt_{\text{now}}}, \quad \beta = 8 \frac{dt_{\text{old}} + dt_{\text{now}}}{7dt_{\text{old}} + 5dt_{\text{now}}}.$$

The local truncation error for u^{n+1} is one order higher than the local truncation errors for u_c^{n+1} and u_f^{n+1} (see Appendix A). Note that if $dt_{\text{now}} = dt_{\text{old}}$ then (18) reduces to the standard Richardson extrapolation formula for second-order schemes.

2.3. Adaptive time-Stepping. The adaptive scheme seeks a time-step dt_{now} such that the (approximate) local truncation error $\epsilon_c^{n+1} \in (tol - range, tol + range)$. In practice, we have used a relationship such as $tol = 10^{-6}$ and $range = tol/3$. The scheme has user-specified parameters: tol , $range$, dt_{min} , dt_{max} , i_{max} , η_{min} , and η_{max} .

1. Set the loop counter, i , to 1 and set $dt^1 = dt_{\text{old}}$, where dt^i is the i^{th} guess at a value for dt_{now} .
2. (a) Take coarse and fine steps to compute u_c^{n+1} and u_f^{n+1} and use (17) to approximate ϵ_c^i . Use the multistep scheme for $n > 1$ and equation (12) with $\omega = 0$ (single-step) for the first time-step.
(b) Compute ϵ_c^i and check if $|\epsilon_c^i - tol| < range$. If yes, go to step 5.
3. Check the loop counter. If i_{max} attempts have been made trying to find an acceptable value for dt_{now} and $|\epsilon_c^i| > tol + range$, then set dt_{now} to dt_{min} . Alternatively, if at any time $dt_{\text{now}} > dt_{\text{max}}$, then set dt_{now} to dt_{max} . Compute the resulting u_c^{n+1} and u_f^{n+1} , and go to step 5.
4. Increment the loop counter by 1 and make a guess at dt_{now} based on equation (19) with $p = 3$ (the order of the local truncation error) and return to step 2

$$(19) \quad dt^{i+1} = dt^i \min \left(\max \left(\left(\frac{tol}{\epsilon_c^i} \right)^{1/p}, \eta_{\text{min}} \right), \eta_{\text{max}} \right)$$

5. Advance in time, setting $dt_{\text{now}} = dt^i$, $t^{n+1} = t^n + dt_{\text{now}}$ and use (18) to define u^{n+1} .

i_{max} is the maximum number of allowed iterations per time-step, and dt_{min} and dt_{max} are the minimum and maximum allowed time-steps, respectively. dt_{min} is set so that the simulation completes in a reasonable period of time; we used values in the range 10^{-10} to 10^{-8} for runs up to around time 50.

Equation (19) is a natural extension of refinement strategies for single step schemes, where p is the order of the local truncation error (LTE). It is based on the idea that the LTE satisfies $\epsilon^i \approx C(dt^i)^p$, so setting $dt^{i+1} = \left(\frac{tol}{\epsilon^i} \right)^{1/p} dt^i$ will bring ϵ^{i+1} closer to tol . The role of η_{min} and η_{max} in (19) is to prevent dt^{i+1} from changing “too much” at once ($\eta_{\text{min}} \leq dt^{i+1}/dt^i \leq \eta_{\text{max}}$). For η_{max} and η_{min} , we used values such as 1.2 and 0.8, respectively, as safeguards to guarantee that the adaptive stepper is able to converge. This type of error control strategy is discussed in Chapter II.4 of Hairer, Norsett and Wanner [50]. Since we’re using a two-step time-stepping scheme, for the first time-step, we use a one-step IMEX scheme, i.e. (12) with $\omega = 0$, which has an LTE $\sim O(dt^2)$ along with error control that uses $p = 2$ in (19) and the extrapolation formula $u^{n+1} = 2u_f - u_c$.

Above, we described the time-stepping for a single ODE according to the steps presented above. Given the system of ODEs that would arise from spatially discretizing a parabolic PDE, we use the same approach but define the local truncation error using the norm of \mathbf{u} . In our simulations, we chose the l^2 norm.

2.4. Spatial Discretization. The geometry is divided into a non-uniform mesh, with $x \in [0, 1]$ and parameterized via

$$(20) \quad x(s) : [0, 1] \rightarrow [0, 1],$$

so that $x_i := x(s_i)$, $0 = x_1 < x_2 < \dots < x_N = 1$ and $dx(i) := x(s_{i+1}) - x(s_i)$ where $s_i = (i-1)ds$, $i = 1, 2, \dots, N$ and $ds = 1/(N-1)$. The function $x(s)$ may, for example,

be piecewise linear with smaller slopes near the endpoints $x = 0, 1$ and a large slope around $x = 1/2$. This would result in a piecewise uniform mesh that is finer near the endpoints. Alternatively, one might use a logistic function, for example, to create a mesh with smoothly varying nonuniformity as in

$$(21) \quad x(s_i) = \begin{cases} 0 & i = 1 \\ \frac{1}{1+e^{-\gamma(s_i-\frac{1}{2})}} & i = 2, \dots, N-1 \\ 1 & i = N. \end{cases}$$

The larger the value of γ , the finer the mesh near the endpoints. In practice, we used a piecewise constant mesh with three or five regions of uniform mesh.

For the discussion of spatial discretization of the parabolic PDE, we refer to a generic continuity equation $u_t = -(J(u, u_x, x))_x$. When applied to (1), $u = c_{\pm}$ and $J(u, u_x, x) = -c_{\pm,x} - z_{\pm} c_{\pm} \phi_x$. The function $u(\cdot, t)$ on the interval is approximated by a vector $\mathbf{u}(t) \in \mathbb{R}^N$ with $u_i(t) \approx u(x_i, t)$. At internal nodes, the flux is approximated using a second-order center-differencing scheme

$$(22) \quad \frac{du_i}{dt} \approx (u_t)|_{x_i} = (J(u, u_x, x))|_{x_i} \approx \frac{J(u, u_x, x)|_{x_{i+1/2}} - J(u, u_x, x)|_{x_{i-1/2}}}{x_{i+1/2} - x_{i-1/2}},$$

where $x_{i+1/2}$ is the midpoint of $[x_i, x_{i+1}]$ and the approximations

$$(23) \quad u_{i \pm 1/2} \approx \frac{u_{i \pm 1} + u_i}{2}, \quad u_x|_{x_{i-1/2}} \approx \frac{u_i - u_{i-1}}{dx_{i-1}}, \quad \text{and} \quad u_x|_{x_{i+1/2}} \approx \frac{u_{i+1} - u_i}{dx_i}$$

are used. At the boundary nodes, we use a three-node, second-order approximation for u_x . For example, the approximation at the left hand boundary is

$$(24) \quad u_x|_{x=0} \approx -\frac{2dx_1 + dx_2}{dx_1(dx_1 + dx_2)} u_1 + \frac{dx_1 + dx_2}{dx_1 dx_2} u_2 - \frac{dx_1}{dx_2(dx_1 + dx_2)} u_3.$$

For the spatial discretization of the elliptic PDE (2) in the interior, we again use a three point center-differencing scheme

$$(25) \quad \frac{2u_{i+1}}{dx_i(dx_i + dx_{i-1})} - \frac{2u_i}{dx_i dx_{i-1}} + \frac{2u_{i-1}}{dx_{i-1}(dx_i + dx_{i-1})} \approx u_{xx}|_{x_i} = f(x_i)$$

where $u = -\phi/\epsilon^2$ and $f = (z_+ c_+ + z_- c_-)/2$. On the boundaries $x = 0, 1$, we use a left or right-handed three point stencil to approximate the first derivatives in the boundary conditions (8)–(9).

Bazant and coworkers (i.e. in [16] and [17]), used a Chebyshev pseudospectral spatial discretization in their work, where we use a finite difference discretization. We wrote and tested a Chebyshev spectral version of the code using the `chebfun` package [51, 52] and found that, while the spectral and finite difference codes gave nearly identical results, the finite difference code ran orders of magnitude faster than the spectral code when using the same time-stepping scheme.

2.5. Boundary Conditions. For the semi-implicit schemes (11) and (12), a natural first approach to the boundary conditions on the flux of c_+ , (4)–(5), would be to handle the linear term of the flux implicitly and to extrapolate both the flux constraint function and the nonlinear term in the flux forward to time t^{n+1} . For the boundary condition (5) this yields

$$(26) \quad -(c_{+,x})_N^{n+1} - (1 + \omega)(c_+ \phi_x)_N^n + \omega(c_+ \phi_x)_N^{n-1} = (1 + \omega) G^n - \omega G^{n-1}$$

where

$$(27) \quad G^n = 4k_{c,c} (c_+)_N^n e^{-0.5 \Delta\phi_{\text{right}}} - 4 j_{r,c} e^{0.5 \Delta\phi_{\text{right}}} \quad \text{with} \quad \Delta\phi_{\text{right}} = v(t^n) - \phi_N^n$$

and G^{n-1} is defined analogously. The boundary conditions (4) and (3) are discretized analogously. The equations for the discretized boundary conditions and the time-stepping equations at the interior nodes are then simultaneously solved for \mathbf{c}_\pm^{n+1} . We refer to this approach as the “direct” method of handling the boundary conditions.

We found that using the “direct method” for boundary conditions yields undesirable properties for the simulation of the PNP-FBV system. For example, the simulation is not second-order accurate in time when the SBDF2 time-stepper (11) is used. Further, we cannot take the tolerance to be arbitrarily small in the VSSBDF2 adaptive time-stepper [26, 53]. For this reason, we used an alternative approach for the boundary conditions. We refer to it as the “ghost point” method (see Section 1.4 of Thomas [54]), since it assumes the PDEs (1) hold at $x = 0, 1$ and uses the same time-stepping scheme as at the internal nodes. Applying the PDEs at x_1 and x_N requires the flux at neighbouring points; in a true ghost point method this flux would be located at “ghost points” outside the computational domain: x_0 and x_{N+1} . Instead, we use the flux at x_1 and x_N ; there are no points outside the computational domain. For example, the spatially discretized PDE for c_+ at $x = 0$ is the ODE

$$(28) \quad \frac{\partial c_+}{\partial t} \Big|_{x=0} = \frac{(c_{+,x} + c_+ \phi_x)|_{x=dx_1/2} - F(t)}{dx_1/2}.$$

For the semi-implicit time-stepping schemes, (11) and (12), we treated the $c_{+,x}$ term implicitly (like g) and extrapolated the $c_+ \phi_x$ and $F(t)$ terms (like f). We found that using the ghost point method for the boundary conditions yields a method that is second-order accurate in time, when the (constant-time-step) SBDF2 time-stepper (11) is used, and the tolerance could be taken to be as small as we desired, near to round-off, in the VSSBDF2 adaptive time-stepper [26, 53].

For the implicit schemes (14)–(15), we used the ghost point method as well. The terms on the right-hand side of (28) were all handled implicitly (like g).

2.6. Time-stepping the Parabolic-Elliptic System. The PNP-FBV system has 2 parabolic PDEs (1), one elliptic PDE (2), and may have one ODE (10). We now describe how to time-step this system in a way that the global truncation error is $O(dt^2)$ when we take constant time-steps ($dt_{\text{old}} = dt_{\text{now}} = dt$). We present the case when a current is imposed and so the ODE (10) needs to be time-stepped along with the PDEs.

2.6.1. Using the Semi-Implicit Schemes SBDF2 and VSSBDF2. The potential ϕ appears in the term $(c_\pm \phi_x)_x$ in (1) and in the boundary conditions (3)–(5). If the semi-implicit schemes SBDF2 (11) or VSSBDF2 (12) are used to time-step the parabolic PDEs then these terms involving ϕ are extrapolated forward; the new concentrations can be computed using the old potentials. The new potential can be then be computed using the new concentrations. Figure 2 presents this splitting scheme for the first and second (and subsequent) time-steps. The initial value $\phi_x(1, 0)$ is denoted ϕ_x^1 and, throughout the article, ϕ_x^n denotes the approximation of $\phi_x(1, t^n)$. The initial data $c_\pm(x, 0)$ is discretized resulting in initial vectors $\mathbf{c}_+^1, \mathbf{c}_-^1 \in \mathbb{R}^N$. Given \mathbf{c}_\pm^1 and ϕ_x^1 , we solve the elliptic PDE to determine $\phi^1 \in \mathbb{R}^N$. Using the one-step semi-implicit scheme (13) on the parabolic PDEs (1) and the ODE (10), we determine \mathbf{c}_\pm^2 and ϕ_x^2 . Given \mathbf{c}_\pm^2 and ϕ_x^2 , we solve the elliptic PDE to determine ϕ^2 . (11) or (12) is

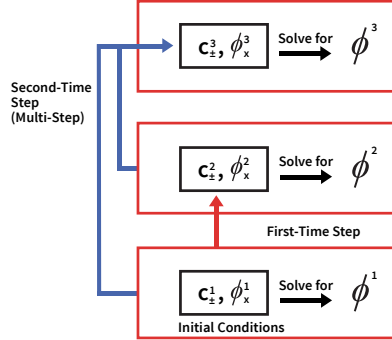


Fig. 2: A diagram of the first three time levels for the semi-implicit schemes. \mathbf{c}_\pm^1 and ϕ_x^1 are the initial conditions, which are used by the elliptic solver to generate ϕ^1 . (Throughout the article, ϕ_x^n denotes the approximation of $\phi_x(1, t^n)$.) \mathbf{c}_\pm^1 , ϕ_x^1 , and ϕ^1 are then used to take a step using (13), creating \mathbf{c}_\pm^2 and ϕ_x^2 . These are then used to generate ϕ^2 . \mathbf{c}_\pm^1 , ϕ_x^1 , ϕ^1 , \mathbf{c}_\pm^2 , ϕ_x^2 , and ϕ^2 are used in a two-step scheme, (11) or (12), to create \mathbf{c}_\pm^3 and ϕ_x^3 which are then used to create ϕ^3 .

then applied to determine \mathbf{c}_\pm^3 and ϕ_x^3 ; ϕ^3 is then solved for, using \mathbf{c}_\pm^3 and ϕ_x^3 . And so forth. It is important that ϕ^{n+1} be solved for using \mathbf{c}_\pm^{n+1} and ϕ_x^{n+1} ; not doing so reduces the global truncation error from $O(dt^2)$ to $O(dt)$. Furthermore, because ϕ^n at time t^n is determined from the other quantities at time t^n the elliptic equation does not factor into the computation of the approximate local truncation error during adaptive time-stepping.

2.6.2. Using the Implicit Schemes BDF2 and VSBDF2. If implicit time-stepping is used, problem is viewed as a system of DAEs and the $3N$ unknowns \mathbf{c}_+^{n+1} , \mathbf{c}_-^{n+1} , and ϕ^{n+1} are simultaneously solved for. If there's an applied current, rather than an applied voltage, then ϕ_x^{n+1} is also solved for, and so there are $3N + 1$ unknowns.

The parabolic PDEs (1) result in $2N$ equations. The ghost-point method uses the Butler-Volmer boundary conditions, (4)–(5) — the fluxes $F(t)$ and $G(t)$ are taken at time t^{n+1} . The elliptic PDE (2) and its boundary conditions (8)–(9) are applied at time t^{n+1} as well; this provides an additional N equations. In the case of current boundary conditions, (10) provides the final required equation.

The $3N$ equations are rewritten as $\mathcal{F}(\mathbf{c}_+, \mathbf{c}_-, \phi) = \vec{0}$ where $\mathcal{F} : \mathbb{R}^{3N} \rightarrow \mathbb{R}^{3N}$; the function \mathcal{F} implicitly depends on the known quantities \mathbf{c}_\pm^n , ϕ^n , \mathbf{c}_\pm^{n-1} , and ϕ^{n-1} . We use the Newton–Raphson method to find approximate solutions of the $3N$ nonlinear equations, thus determining \mathbf{c}_+^{n+1} , \mathbf{c}_-^{n+1} , and ϕ^{n+1} . We extrapolate the previous solutions to provide a first guess: $(1 + \omega)\phi^n - \omega\phi^{n-1}$ and so forth. If a current is imposed then the natural generalization is made to determine the $3N + 1$ unknowns.

We stopped the iterations when $\|\mathcal{F}(\mathbf{c}_+, \mathbf{c}_-, \phi)\| < 10^{-10}$; we found that the average value of $\|\mathcal{F}\|$ at the final iterate was 10^{-11} . For comparison, when we used MATLAB's `fsolve` routine, rather than our Newton–Raphson subroutine, the code ran slightly slower and the average value of $\|\mathcal{F}\|$ at the final iterate continued to be 10^{-11} .

3. Simulations of the PNP-FBV Equations. Table 1 presents the results from convergence testing performed on the PNP-FBV system using both the SBDF2

and BDF2 numerical schemes. For these convergence tests, we considered current, rather than voltage boundary conditions, which requires time-stepping the additional ODE (10). The results demonstrate that both schemes are at least second-order accurate.

dt	Ratios (SBDF2)	Ratios (BDF2)
0.00005	4.0951	4.0720
0.00005/2	4.0504	4.0348
0.00005/4	4.0260	4.0170
0.00005/8	4.0132	4.0084
0.00005/16	4.0066	4.0042

Table 1: Convergence tests on PNP-FBV system (1)–(9) with current boundary conditions (10) and an imposed external current $j_{\text{ext}} = 0.5$. All model parameters were set to 1 except $\epsilon = 0.01$. For each method, we compute seven solutions on a uniform mesh $dx = 1/30$ up to time $T = .001$, using equation (13) for the first time-step of the SBDF2 scheme and equation (16) for the first time-step of the BDF2 scheme. The i^{th} solution, denoted $\mathbf{u}_i = [\mathbf{c}_{+,i}; \mathbf{c}_{-,i}]$, is computed using $dt = 0.0001/2^i$. That is $\mathbf{u}_i \in \mathbb{R}^{2(N+1)} \times \mathbb{R}^{n_i}$ where $n_i = 10 \times 2^i + 1$ and $\mathbf{u}_i^{n_i} \in \mathbb{R}^{2(N+1)}$ approximates the solution at the final time T . The discrete solutions \mathbf{u}_i at the final time $T = .001$ are used to define the ratios: $\|\mathbf{u}_i^{n_i} - \mathbf{u}_{i+1}^{n_{i+1}}\|/\|\mathbf{u}_{i+1}^{n_{i+1}} - \mathbf{u}_{i+2}^{n_{i+2}}\|$ with the l^2 norm. Ratios approaching 4 indicate second order accuracy in time. While we only show 5 values of dt in the table, runs with $dt = 0.00005/32$ and $dt = 0.00005/64$ were necessary to create the ratios.

As discussed in the companion paper [1], the addition of a Richardson extrapolation step provides a stabilizing effect to the time-stepper, which, though valuable in practice, is not useful in demonstrating the stability constraints of the VSSBDF2 scheme. Therefore, unless noted otherwise, the simulations presented in the rest of this section do not use Richardson extrapolation in the adaptive time-stepper. Specifically, in step 5 described in Subsection 2.3, u^{n+1} was taken to equal u_c^{n+1} .

Figure 3 considers an initial value problem for the PNP-FBV system (1)–(9) with constant imposed voltage. The initial data is fixed, as are all the other physical parameters. Solutions are computed using the VSSBDF2 adaptive time-stepper (left plot) and using the VSBDF2 adaptive time-stepper (right plot).

The top figure on the left demonstrates that, after a short transient, the solution found by the VSSBDF2 adaptive time-stepper initially decays exponentially quickly to a numerical steady state. However, once the solution is within (approximately) 10^{-7} of the steady-state solution, this convergence ends and the computed solution stays about 10^{-7} away from the steady state. The middle figure on the left demonstrates that the VSSBDF2 adaptive time-stepper is keeping the (approximate) local truncation error (17) within the user-specified range of $(\text{tol} - \text{range}, \text{tol} + \text{range})$. The bottom figure on the left demonstrates that the time-step size initially increases exponentially fast and after a while it decreases and stabilizes; we denote the value that it stabilizes to as dt_∞ . The dashed line in the bottom figure on the left is the stability threshold found by the linear stability analysis presented in Section 4 of the companion article [1]; we denote this value as dt^* . This simulation demonstrates that the VSSBDF2 adaptive time-stepper appears to eventually stabilize at a time-step size that is precisely the stability threshold. The top left plot presents the deviation from the numerical steady state $\mathbf{c}_{+,ss}$. The numerical steady state, $\mathbf{c}_{\pm,ss}$ and ϕ_{ss} , satisfies the discretized version of $0 = c_{\pm,xx} + z_{\pm}(c_{\pm}\phi_x)$ and (2). The numerical steady state was found by first computing an initial value problem using the VSSBDF2 adaptive time-stepper and then repeating the computation using the SBDF2 time-stepper with a (fixed) time-step size that is less than the value dt_∞ found by

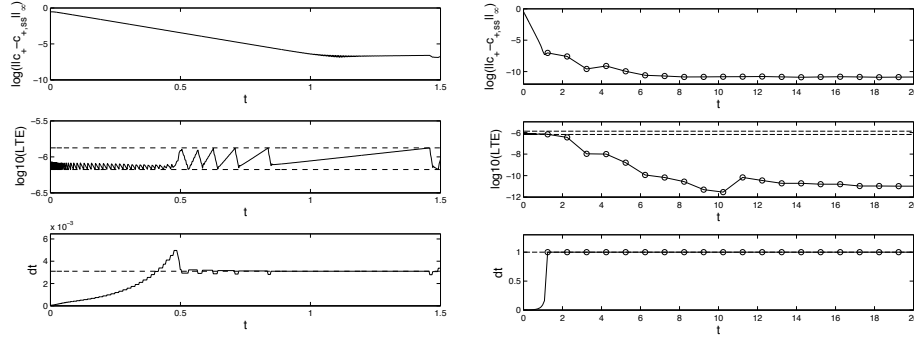


Fig. 3: PNP-FBV system (1)–(9) with constant voltage $v(t) = 2$, $\epsilon = .05$, and all other physical parameters set to 1. The initial data is $c_{\pm}(x, 0) = 1 + .1 \sin(2\pi x)$ and $\phi_x(1, 0) = 0$. For the simulation, $N = 90$, $L_1 = L_2 = L_3 = 1/3$, with $tol = 10^{-6}$, $range = tol/3$, and $dt_{max} = 1$. In the three plots on the left side of the figure, the (implicit-explicit) VSSBDF2 adaptive time-stepper is used, and in the three plots on the right hand of the figure, the (fully implicit) VSBD2 time-stepper is used. Note that in the right plots, circle markers are used after the time-step size dt reaches dt_{max} , and also that the left plots shows data up to $t = 1.5$, where the right plots show data up to $t = 20$. Top plot: The logarithm of the maximum deviation of the computed solution c_+ from the steady state $c_{+,ss}$ at each moment in time: $\log(\|c_+^n - c_{+,ss}\|_\infty)$. Deviations of c_- and ϕ from the corresponding steady state profiles behave similarly. Middle plot: The logarithm of the approximate local truncation error, (17). The dashed lines in both plots indicate $\log(tol \pm range)$. Bottom plot: Time-step size, dt , plotted versus time. The dashed line in the left plot indicates the stability threshold $dt^* = 3.1000 \cdot 10^{-3}$ computed using the linear stability analysis presented in Section 4 of the companion paper [1]. The dashed line in the right plot indicates the maximum step-size dt_{max} .

the adaptive time-stepper. We find that a long-time simulation using fixed time-steps results in a solution that relaxes to a steady-state solution as long as the time-steps are taken to be smaller than dt_∞ . We use the solution at a late time as the numerical steady-state solution. If one then plots the logarithm of the deviation of the SBDF2 solutions from this steady state, one sees exponentially fast convergence in time and with the deviation decreasing approximately to round-off (10^{-14}).

The plots to the right in Figure 3 used the adaptive time-stepper based on the fully implicit VSBD2 scheme (15). The bottom plot on the right demonstrates that the time-step increases exponentially until it reaches the user-specified dt_{max} ; the time-step is held at this value for the duration of the simulation. The middle plot on the right demonstrates that the (approximate) local truncation error stays within the user-specified range of $(tol - range, tol + range)$ until the time when the time-step is held fixed at dt_{max} . Once the time-step is held fixed at dt_{max} , the error control mechanism is no longer in play — the local truncation error begins to decay to around 10^{-11} and then stays around this value. Similarly, the top plot on the right demonstrates that the deviation from the steady state initially decreases exponentially fast, lingers around 10^{-7} for a bit, and then decreases to around 10^{-11} . The deviations don't decrease to 10^{-14} as they did for the SBDF2 simulation because the VSBD2 adaptive time-stepper uses an iterative nonlinear solver and this solver is only solving the equations up to a tolerance of about 10^{-11} .

We find that we need to handle the full DAE system implicitly. Specifically, if we use a scheme in which the parabolic PDEs are stepped with the fully implicit

method (VSBD2) but the elliptic PDE is stepped using the semi-implicit method (VSSBDF2) then the observed behaviour is similar to that shown in the plots to the left in Figure 3. This is in contrast with some other work; for example in [55] the authors have a nonlinear diffusion equation they time-step using BDF methods however they extrapolate the diffusivity coefficient forward in time, to avoid the need for a nonlinear solve, but find that their time-stepper remains unconditionally stable.

3.1. Parameter choice and observed numerical behaviour. When computing solutions of the PNP-FBV system with time-independent voltage or current, we find that if we use the SBDF2 time-stepper with (fixed) $dt > dt^*$ then, after a transient, the computed solutions grow exponentially fast. If we use a (fixed) $dt < dt^*$ then, after a transient, the solution eventually converges exponentially fast to the steady state and the local truncation error decays exponentially fast to zero (round-off).

If, instead, we use the VSSBDF2 adaptive time-stepper then as the solution starts to converge to the steady state, the time-steps are taken larger and larger in order to keep the local truncation error within the interval $(tol - range, tol + range)$. If the maximum allowed time-step size, dt_{\max} , is smaller than dt^* then there is no thresholding due to numerical instability; in this case, dt increases to dt_{\max} and is then held constant and the local truncation error is no longer constrained to stay in the interval $(tol - range, tol + range)$. As a result, the solution continues to converge to the steady state and the local truncation error decays exponentially to zero. If, however, $dt_{\max} > dt^*$ then once the time-step size increases past dt^* , the unstable eigenmode(s) of the underlying linearized problem start to grow exponentially and this growth stops the solution from converging to the steady state. It may happen that the time-step size transiently reaches and is held at dt_{\max} in which case the local truncation error may transiently decrease below $tol - range$.

3.2. Response to Time-dependent Forcing. We next considered the PNP-FBV system with time-dependent voltage boundary conditions. The voltage was chosen to be nearly piecewise constant in time; there are fast steps in the voltage at three times as shown in the left plot of Figure 4. Before the first voltage step, the solution is relaxing to the steady state corresponding to zero voltage. After this voltage step, the solution relaxes to the steady state corresponding to $v(t) = 1$. After each voltage step, the solution relaxes to the relevant steady state. The time-steps chosen by the VSSBDF2 adaptive stepper are shown in the right plot of Figure 4. After an initial transient, where the time-steps are as small as 10^{-6} , the time-steps stabilize. In response to each voltage step, the time-steps decrease by several orders of magnitude after which they stabilize. This is a demonstration of the value of adaptive time-stepping versus constant time-steps: a constant step method would require step sizes of 10^{-5} to resolve the imposed voltage $v(t)$ used here, whereas the VSSBDF2 adaptive stepper has step sizes larger than 10^{-2} for most of the duration of the simulation and the VSBD2 adaptive stepper has time-steps that can reach dt_{\max} if there is a large enough time between sudden changes in the the voltage or current.

In all of our simulations, we found that if there was a sufficiently long period of time during which either the voltage or the current were held constant then the solution would converge to the corresponding steady state and the time-step sizes would stabilize to a limiting value, which we denote by dt_{∞} . (To approximate dt_{∞} , we average 100 sequential time-steps at the end of the period of constant voltage/current.) As Figure 4 demonstrates, dt_{∞} depends on the applied voltage (or on the applied

current). We also found that dt_∞ does not depend on the parameters tol and $range$ in the adaptive timestepper.

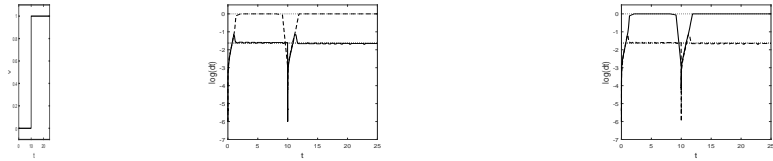


Fig. 4: PNP-FBV system (1)–(9) with uniform mesh $dx = 1/90$, $tol = 1e-6$, $range = tol/3$, all model parameters set to 1 except $\epsilon = 0.5$. The initial data for the concentrations is $c_\pm(x, 0) = 1 + .1 \sin(2\pi x)$. The left plot shows the time-dependent voltage $v(t)$. The voltage is a sharp transition from 0 to 1 at time $t = 10$, modeled by the equation $v(t) = (\tanh(1000(t - 10)) + 1)/2$. The centre plot presents the time-step sizes as a function of time for the implicit-explicit scheme (solid line) and the fully implicit scheme (dashed line). The right plot presents the time step sizes as a function of time for the fully implicit scheme (solid line) and the implicit-explicit scheme (dashed line). The dotted lines in the centre and right figures correspond to $dt^* = 0.0250, 0.0223, 0.0191$, and 0.0158 ; they are the stability thresholds found using the linear stability analysis presented in Section 4 of the companion paper.

3.3. Effect of the Singular Perturbation Parameter. Next, we consider the singular perturbation parameter, ϵ , which controls the dynamics of the boundary layers near the electrodes in the PNP-FBV system (2). Figure 5 presents some steady-state solutions for PNP-FBV system (1)–(9) with current boundary conditions (10). The figure on the left presents the steady-state concentration of the positive species, $c_+(x)$, for three values of ϵ . The smaller the value of ϵ , the thinner the transition layer near $x = 0$ and $x = 1$ is. The figure on the right presents the corresponding steady-state potential, $\phi(x)$. For relatively small values of ϵ , we found that if one decreases ϵ by a factor of a then the limiting time-step size, dt_∞ , decreases by roughly a^2 ; see Table 2.

By taking small enough time-steps, the VSSBDF2 adaptive time-stepper is able to run with small values of ϵ . Furthermore, although it is more computationally expensive, the VSBDF2 adaptive time-stepper is able to take arbitrarily large time-steps for equilibrated solutions, regardless of the value of ϵ . Previous work on time-dependent solutions to the PNP-FBV system [23, 56] took comparably large values, $\epsilon \geq 10^{-3}$, whereas in principle we are able to simulate with any value of ϵ . The adaptiveness of the time-stepper allowed us to numerically explore certain standard experimental protocols, such as linear sweep voltammetry, in which a time-dependent voltage or current is applied [57].

4. Conclusions and Future Work. In this work, we considered the Poisson-Nernst-Planck equations with generalized Frumkin-Butler-Volmer reaction kinetics

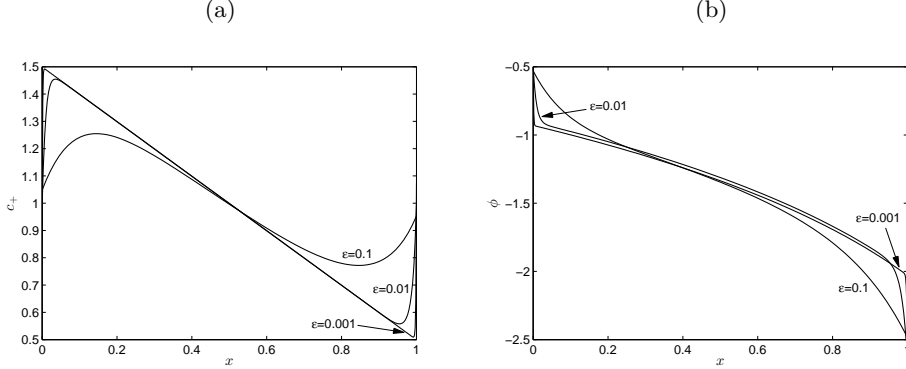


Fig. 5: Steady-state solutions for PNP-FBV system (1)–(9) with current boundary conditions (10). The imposed external current is $j_{\text{ext}}(t) = 0.5$. The simulations were run until time $t = 5$; the profiles at that time are shown here. Three values of ϵ were used. For $\epsilon = 0.1, 0.01$, a uniform-in-space mesh was used with $dx = 1/90$. For $\epsilon = 0.001$, a piecewise uniform-in-space mesh was used with $dx = 1/600$ in $[0, 0.1]$ and $[0.9, 1]$ and $dx = 1/75$ in $[0.1, 0.9]$. Left figure: concentration of positive species, c_+ , versus x . Right figure: potential, ϕ , versus x .

ϵ	dt_∞	dt_∞/ϵ^2
0.1	0.0257	2.57
0.01	0.000241	2.41
0.001	3.70×10^{-6}	3.70
10^{-4}	2.48×10^{-8}	2.48
10^{-5}	2.25×10^{-10}	2.25
10^{-6}	2.37×10^{-12}	2.37

Table 2: The PNP-FBV system (1)–(9) are simulated with the applied voltage $v(t) = 0$. Six values of ϵ are considered. We denote the limiting timestep chosen by the VSSBDF2 adaptive stepper by dt_∞ . dt_∞ was computed by averaging the time-step sizes over 100 sequential time-steps chosen late in the simulation.

at the electrodes. We developed a solver that dynamically chooses the time-step size so that the local truncation error is within user-specified bounds. The spatial discretization can be nonuniform, allowing for the finer mesh needed near the electrodes to resolve the boundary layers. Adaptive time-stepping allows the solver to choose small time-steps during the initial transient period during which the boundary layers may be forming quickly in response to the boundary conditions, and also allows one to more efficiently study physical situations in which the imposed voltage or current have sudden, fast changes.

We considered two adaptive time-stepping schemes in this work. The implicit-explicit VSSBDF2 scheme was shown to have a stability constraint which causes its time-step sizes to stabilize to a limiting value in the long-time limit of constant voltage or current, whereas the fully implicit VSBDF2 time-stepper was found to have no such stability constraint. However, the fully implicit scheme requires a computationally expensive nonlinear solve at each time-step, resulting in far longer computation time per step. The stability behaviour of the implicit-explicit scheme can be understood

by linearizing the numerical scheme about the steady state, and is fully explored in the companion article [1].

As demonstrated in Table 2, the constraint on the time-step size for VSSBDF2 is roughly on the order of ϵ^2 as $\epsilon \rightarrow 0$. This implies that there will be a break-even point. In some regimes the VSSBDF2 scheme will be faster while in other regimes the VSBDF2 scheme will be faster despite being significantly slower per time-step.

Appendix A. Derivation of the Local Truncation Error Formula and the Extrapolation Formula.

In this appendix, the error approximation and extrapolation formula used in Subsection 2.2 is derived. We consider time-stepping the ODE $du/dt = f(u) + g(u)$ where the value of u at time $n+1$ is given by (12). Making the substitutions $u^{n+1} = u(t + dt_{\text{now}})$ and $u^{n-1} = u(t - dt_{\text{old}})$ and performing a multivariable Taylor expansion about t , the local truncation error is found to take the form

$$\begin{aligned} LTE = & (u'(t) - f(u(t)) - g(u(t))) dt_{\text{now}} + (u''(t) - f'(u(t)) u'(t) - g'(u(t)) u'(t)) dt_{\text{now}}^2 \\ & + \left(\frac{1}{2} f''(u(t)) u'(t)^2 + \frac{1}{2} f'(u(t)) u''(t) - \frac{1}{6} u^{(3)}(t) \right) dt_{\text{old}} dt_{\text{now}}^2 \\ (29) \quad & + \left(-\frac{1}{2} g''(u(t)) u'(t)^2 - \frac{1}{2} g'(u(t)) u''(t) + \frac{1}{3} u^{(3)}(t) \right) dt_{\text{now}}^3 + O(dt^4) \end{aligned}$$

where $O(dt^4)$ denotes terms where dt_{now} and dt_{old} combined appear four or more times. If $u(t)$ is a thrice-differentiable solution, the dt_{now} and dt_{now}^2 terms vanish and the cubic term can be simplified, resulting in

$$\begin{aligned} LTE = & \left(\frac{1}{2} f''(u(t)) u'(t)^2 + \frac{1}{2} f'(u(t)) u''(t) - \frac{1}{6} u^{(3)}(t) \right) dt_{\text{old}} dt_{\text{now}}^2 \\ (30) \quad & + \left(-\frac{1}{2} g''(u(t)) u'(t)^2 - \frac{1}{2} g'(u(t)) u''(t) + \frac{1}{3} u^{(3)}(t) \right) dt_{\text{now}}^3 + O(dt^4) \\ (31) \quad & = \left(\frac{1}{3} u^{(3)}(t) - \frac{1}{2} g''(u(t)) u'(t)^2 - \frac{1}{2} g'(u(t)) u''(t) \right) dt_{\text{now}}^2 (dt_{\text{now}} + dt_{\text{old}}) + O(dt^4). \end{aligned}$$

This means that if $u^{(3)}(t)$ is bounded, the local truncation error for the coarse step is

$$(32) \quad \epsilon_c = u_c^{n+1} - u(t^{n+1}) \approx C dt_{\text{now}}^2 (dt_{\text{now}} + dt_{\text{old}})$$

To find the local truncation error for u_f^{n+1} , we find the local truncation error for $u_f^{n+\frac{1}{2}}$ by replacing dt_{now} and dt_{old} in (32) by $\frac{dt_{\text{now}}}{2}$ and $\frac{dt_{\text{old}}}{2}$, respectively. We then find the local truncation error for u_f^{n+1} by setting both dt_{now} and dt_{old} to $\frac{dt_{\text{now}}}{2}$. Adding these local truncation errors yields the LTE for u_f^{n+1} ,

$$(33) \quad \epsilon_f = u_f^{n+1} - u(t^{n+1}) \approx \frac{C dt_{\text{now}}^2 (dt_{\text{now}} + dt_{\text{old}})}{8} + C \frac{dt_{\text{now}}^3}{4}$$

Using equations (32) and (33), we can approximate C using u_c , u_f , dt_{now} and dt_{old} and then use this approximation in (32), resulting in

$$(34) \quad \epsilon_c \approx \frac{u_c - u_f}{\frac{5}{8} dt_{\text{now}}^3 + \frac{7}{8} dt_{\text{now}}^2 dt_{\text{old}}} dt_{\text{now}}^2 (dt_{\text{now}} + dt_{\text{old}})$$

Finally, we subtract ϵ_c from u_c^{n+1} to create a more accurate approximation of $u(t^{n+1})$. This results in the extrapolation formula $u(t^{n+1}) \approx u_c^{n+1} - \epsilon_c = \alpha u_c^{n+1} + \beta u_f^{n+1}$ where

$$(35) \quad \alpha = -\frac{dt_{\text{old}} + 3dt_{\text{now}}}{7dt_{\text{old}} + 5dt_{\text{now}}}, \quad \beta = 8 \frac{dt_{\text{old}} + dt_{\text{now}}}{7dt_{\text{old}} + 5dt_{\text{now}}}.$$

We note that if the time-stepping scheme is fully-implicit, this corresponds to setting $f(u) = 0$ in the above. In this case, (31) is replaced by

$$LTE = -\frac{1}{6} (g''(u(t)) u'(t)^2 + g'(u(t)) u''(t)) dt_{\text{now}}^2 (dt_{\text{now}} + dt_{\text{old}}) + O(dt^4)$$

but there are no resulting changes to equations (32)–(35).

Appendix B. Acknowledgements. We thank Greg Lewis and Steven Ruuth for helpful conversations and encouragement.

REFERENCES

- [1] David Yan, Mary C. Pugh, and Francis P. Dawson. A study of the numerical stability of an imex scheme with application to the Poisson-Nernst-Planck equations, 2019.
- [2] P. M. Biesheuvel and M. Z. Bazant. Nonlinear dynamics of capacitive charging and desalination by porous electrodes. *Phys. Rev. E*, 81(3):031502, 2010.
- [3] P. M. Biesheuvel, Yeqing Fu, and M. Z. Bazant. Diffuse charge and Faradaic reactions in porous electrodes. *Phys. Rev. E*, 83(6):061507, 2011.
- [4] P. M. Biesheuvel, Yeqing Fu, and M. Z. Bazant. Electrochemistry and capacitive charging of porous electrodes in asymmetric multicomponent electrolytes. *Russian J. Electrochem.*, 48(6):580–591, 2012.
- [5] P. B. Peters, R. van Roij, Martin Z. Bazant, and P. M. Biesheuvel. Analysis of electrolyte transport through charged nanopores. *Phys. Rev. E*, 93:053108, 2016.
- [6] Ian Streeter and Richard G. Compton. Numerical simulation of potential step chronoamperometry at low concentrations of supporting electrolyte. *J. Phys. Chem. C*, 112(35):13716–13728, 2008.
- [7] Richard G. Compton and Craig E. Banks. *Understanding Voltammetry*. Imperial College Press, London, 2011.
- [8] E. Victoria Dydek and Martin Z. Bazant. Nonlinear dynamics of ion concentration polarization in porous media: The leaky membrane model. *AIChE Journal*, 59(9):3539–3555, 2013.
- [9] Victor V. Nikonenko, Natalia D. Pismenskaya, Elena I. Belova, Philippe Sistat, Patrice Huguet, Gérald Pourcelly, and Christian Larchet. Intensive current transfer in membrane systems: Modelling, mechanisms and application in electrodialysis. *Adv. Colloid Interface Sci.*, 160(1):101–123, 2010.
- [10] A. Yaroshchuk. Over-limiting currents and deionization shocks in current-induced polarization: local equilibrium analysis. *Adv. Colloid Interface Sci.*, 183:68–81, 2012.
- [11] Martin Z. Bazant and Todd M. Squires. Induced-charge electrokinetic phenomena. *Current Opinion in Colloid & Interface Science*, 15(3):203–213, 2010.
- [12] Martin Z. Bazant, Mustafa Sabri Kilic, Brian D. Storey, and Armand Ajdari. Towards an understanding of induced-charge electrokinetics at large applied voltages in concentrated solutions. *Advances in colloid and interfacial science*, 152(1):48–88, 2009.
- [13] Martin Z. Bazant, Brian D. Storey, and Alexei A. Kornyshev. Double layer in ionic liquids: Overscreening versus crowding. *Phys. Rev. Lett.*, 106(4):046102, 2011.
- [14] Alexei A. Kornyshev. Double-layer in ionic liquids: Paradigm change? *J. Phys. Chem. B*, 111:5545–5557, 2007.
- [15] Martin Z. Bazant, Kevin T. Chu, and B. J. Bayly. Current-voltage relations for electrochemical thin films. *SIAM J. Appl. Math.*, 65(5):1463–1484, 2005.
- [16] Kevin T. Chu and Martin Z. Bazant. Electrochemical thin films at and above the classical limiting current. *SIAM J. Appl. Math.*, 65(5):1485–1505, 2005.
- [17] P. M. Biesheuvel, M. van Soestbergen, and M. Z. Bazant. Imposed currents in galvanic cells. *Electrochimica Acta*, 54:4857–4871, 2009.
- [18] P. Maarten Biesheuvel, Alejandro A. Franco, and Martin Z. Bazant. Diffuse charge effects in fuel cell membranes. *J. Electrochem. Soc.*, 156(2):B225–B233, 2009.

- [19] Alpha A Lee, Svyatoslav Kondrat, Gleb Oshanin, and Alexei A Kornyshev. Charging dynamics of supercapacitors with narrow cylindrical nanopores. *Nanotechnology*, 25(31):315401, 2014.
- [20] Martin Z. Bazant. Theory of chemical kinetics and charge transfer based on nonequilibrium thermodynamics. *Accounts of Chemical Research*, 46(5):1144–1160, 2013.
- [21] M. van Soestbergen. Frumkin-Butler-Volmer theory and mass transfer in electrochemical cells. *Russian Journal of Electrochemistry*, 48(6):570–579, 2012.
- [22] A. A. Moya, J. Castilla, and J. Horro. Ionic transport in electrochemical cells including electrical double-layer effects. A network thermodynamics approach. *J. Phys. Chem.*, 99:1292–1298, 1995.
- [23] M. van Soestbergen, P. M. Biesheuvel, and M. Z. Bazant. Diffuse-charge effects on the transient response of electrochemical cells. *Phys. Rev. E*, 81(2):1–13, 2010.
- [24] Allen J. Bard and Larry R. Faulkner. *Electrochemical Methods: Fundamentals and Applications*. John Wiley & Sons, New York, 2001.
- [25] John Newman and Karen E. Thomas-Alyea. *Electrochemical Systems*. John Wiley & Sons, Hoboken, NJ, 2012.
- [26] David Yan. *Macroscopic Modeling of a One-Dimensional Electrochemical Cell Using the Poisson-Nernst-Planck Equations*. PhD thesis, University of Toronto, 2017.
- [27] John Newman and William H. Smyrl. The polarized diffuse double layer. *Trans. Faraday Soc.*, 61:2229–2237, 1965.
- [28] William H. Smyrl and John Newman. Double layer structure at the limiting current. *Trans. Faraday Soc.*, 63:207–216, 1966.
- [29] Martin Z. Bazant, Katsuyo Thornton, and Armand Ajdari. Diffuse-charge dynamics in electrochemical systems. *Phys. Rev. E*, 70(2):021506, 2004.
- [30] H. Cohen and J. W. Cooley. The numerical solution of the time-dependent Nernst-Planck equations. *Biophys. J.*, 5(2):145–162, 1965.
- [31] James R. Sandifer and Richard P. Buck. An algorithm for simulation of transient and alternating current electrical properties of conducting membranes, junctions and one-dimensional, finite galvanic cells. *J. Phys. Chem.*, 79(4):384–392, 1975.
- [32] Timothy R. Brumleve and Richard P. Buck. Numerical solution of the Nernst-Planck and Poisson equation system with applications to membrane electrochemistry and solid state physics. *J. Electroanal. Chem. Interfacial Electrochem.*, 90(1):1–31, 1978.
- [33] Tomasz Sokalski, Peter Lingenfelter, and Andrzej Lewenstein. Numerical solution of the coupled Nernst-Planck and Poisson equations for liquid junction and ion selective membrane potentials. *J. Phys. Chem. B*, 107(11):2443–2452, 2003.
- [34] W. D. Murphy, J. A. Manzanares, S. Mafé, and H. Reiss. Numerical simulation of the nonequilibrium diffuse double layer in ion-exchange membranes. *J. Phys. Chem.*, 97(32), 1993.
- [35] G. W. Gear. *Numerical Initial Value Problems in Ordinary Differential Equations*. Prentice Hall, Englewood Cliffs, NJ, 1971.
- [36] Donald L. Scharfetter and Herman K. Gummel. Large-signal analysis of a silicon read diode oscillator. *IEEE Trans. Electron Devices*, 16(1):64–77, 1969.
- [37] Silvano Erlicher, Luca Bonaventura, and Oreste S. Bursi. The analysis of the generalized-method for non-linear dynamic problems. *Comput. Mechanics*, 28(2):83–104, 2002.
- [38] Dieter Britz and Jörg Strutwolf. Several ways to simulate time dependent liquid junction potentials by finite differences. *Electrochimica Acta*, 137:328–335, 2014.
- [39] Dieter Britz. *Digital Simulation in Electrochemistry*. Springer, Berlin, 2005.
- [40] Richard G. Compton, Eduardo Laborda, and Kristopher R. Ward. *Understanding Voltammetry: Simulation of Electrode Processes*. Imperial College Press, London, 2014.
- [41] D. Wang and S. J. Ruuth. Variable step-size implicit-explicit linear multistep methods for time-dependent partial differential equations. *Journal of Computational Mathematics*, 26(6):838–855, 2008.
- [42] O. Axelsson, X. He, and M. Neytcheva. Numerical solution of the time-dependent Navier-Stokes equation for variable density-variable viscosity. part I. Technical report, Uppsala University, 2014.
- [43] Daniel Lecoanet, Josiah Schwab, Eliot Quataert, Lars Bildsten, F. X. Timmes, Keaton J. Burns, Geoffrey M. Vasil, Jeffrey S. Oishi, and Benjamin P. Brown. Turbulent chemical diffusion in convectively bounded carbon flames. *Astrophys. J.*, 832(1):71, 2016.
- [44] Gunilla Linde, Jonas Persson, and Lina Von Sydow. A highly accurate adaptive finite difference solver for the Black-Scholes equation. *Int. J. Comp. Math.*, 86(12):2104–2121, 2009.
- [45] J. Rosam, P. K. Jimack, and A. Mullis. A fully implicit, fully adaptive time and space discretisation method for phase-field simulation of binary alloy solidification. *J. Comput. Phys.*, 225(2):1271–1287, 2007.

- [46] S. Eckert, H. Baaser, D. Gross, and O. Scherf. A BDF2 integration method with step size control for elasto-plasticity. *Comput. Mech.*, 34(5):377–386, 2004.
- [47] Roger Peyret. *Spectral Methods for Incompressible Viscous Flow*. Springer-Verlag, New York, 2002.
- [48] Michel Crouzeix. Une méthode multipas implicite-explicite pour l'approximation des équations d'évolution paraboliques. *Numer. Math.*, 35(3):257–276, 1980.
- [49] U. M. Ascher, S. J. Ruuth, and B. T. R. Wetton. Implicit-explicit methods for time-dependent partial differential equations. *SIAM Journal on Numerical Analysis*, 32(3):797–823, 1995.
- [50] Ernst Hairer, Syvert P Nørsett, and Gerhard Wanner. *Solving Ordinary Differential Equations I: Nonstiff Problems (Springer Series In Computational Mathematics)*. Springer Berlin, Heidelberg, 2009.
- [51] Lloyd N. Trefethen. *Approximation Theory and Approximation Practice*. SIAM, 2013.
- [52] Rodrigo B. Platte and Lloyd N. Trefethen. Chebfun: a new kind of numerical computing. In *Progress in Industrial Mathematics at ECMI 2008*, pages 69–87, 2008.
- [53] David Yan, Mary C. Pugh, and Francis P. Dawson. A variable step size implicit-explicit scheme for the solution of the Poisson-Nernst-Planck equations, 2017.
- [54] J. M. Thomas. *Numerical Partial Differential Equations: Finite Difference Methods*. Springer, New York, 1995.
- [55] Oscar P. Bruno and Edwin Jimenez. Higher-Order Linear-Time Unconditionally Stable Alternating Direction Implicit Methods for Nonlinear Convection-Diffusion Partial Differential Equation Systems. *Journal of Fluids Engineering — Transactions of the ASME*, 136(6), JUN 2014.
- [56] Laurits Højgaard Olesen, Martin Z. Bazant, and Henrik Bruus. Strongly nonlinear dynamics of electrolytes in large ac voltages. *Phys. Rev. E*, 82(1):011501, 2010.
- [57] David Yan, Martin Z. Bazant, P. M. Biesheuvel, Mary C. Pugh, and Francis P. Dawson. Theory of linear sweep voltammetry with diffuse charge: Unsupported electrolytes, thin films, and leaky membranes. *Phys. Rev. E*, 95:033303, Mar 2017.